Supplementary Information for "Mechanics of biomimetic 4D printed structures"

W.M. van Rees, E.A. Matsumoto, A.S. Gladman, J.A. Lewis and L. Mahadevan

S1 Validation

Here we show a validation involving the growth of a monolayer annulus into a hemisphere, which has been considered semi-analytically in [1]. In particular, the metric of a spherical shell is prescribed onto a planar annulus plate. As a consequence, the plate will adopt a buckled state that balances stretching and bending energy: zero stretching energy is obtained when the mid-surface fully adopts the spherical geometry, whereas zero bending energy is achieved when the plate remains flat. Consequently, the minimum-energy embedding will strongly depend on the thickness of the plate.

We solve the minimum-energy embedding for a range of thicknesses, and compute the stretching and bending energy for each thickness. As in [1], we set the inner and outer radius of the annulus to, respectively, $R_i = 0.1$ and $R_o = 1.1$. Our geometry is discretised using 33 796 triangles. We compute the energy equilibrium with $Y = 1 \times 10^6$ and $\nu = 0.5$, and report the normalised energy $\tilde{E}/h = 4E(1-\nu^2)/(Y\pi h)$ as in [1]. The results are presented in figure S1, and show excellent agreement with the reference results.

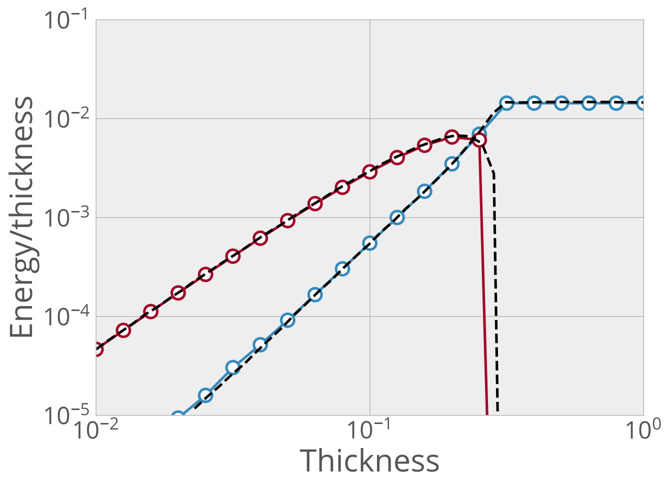

Figure S1: Stretching (blue) and bending (red) energies for the minimal-energy states of planar annuli with prescribed metrics corresponding to a sphere, as a function of the plate thickness. Reference results from [1] are shown in black (dashed).

S2 Print paths and initial conditions

On the following pages, we show large images of the input print path from [2], and the density field and filament-tangent field computing using our model, for each of the five shapes discussed in the main text.

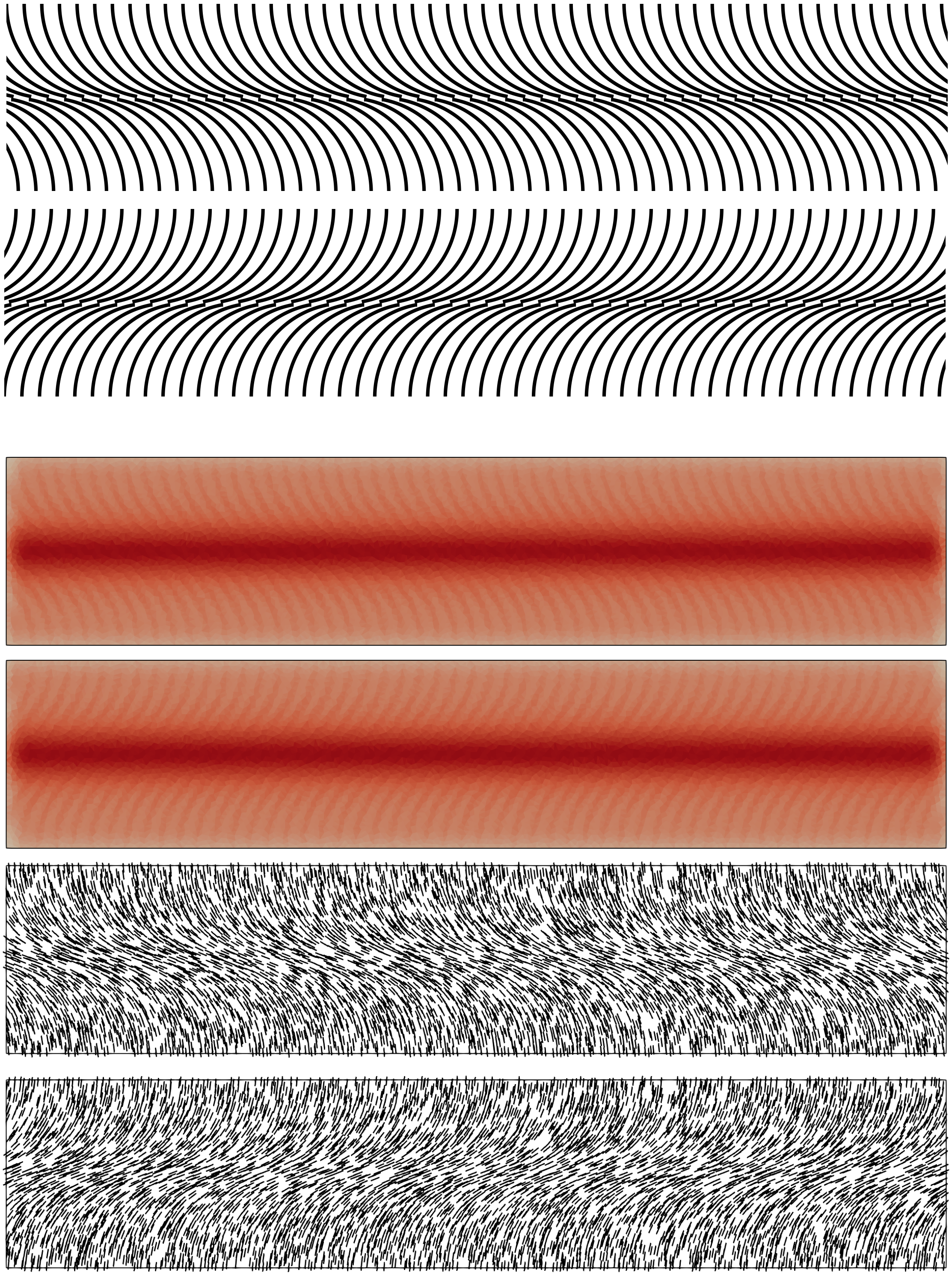

Figure S2: Details of the helicoid. For each of the bottom/top layer, we show the experimental print path (top), the numerical density field (middle) and the numerical filament-tangential growth direction (bottom).

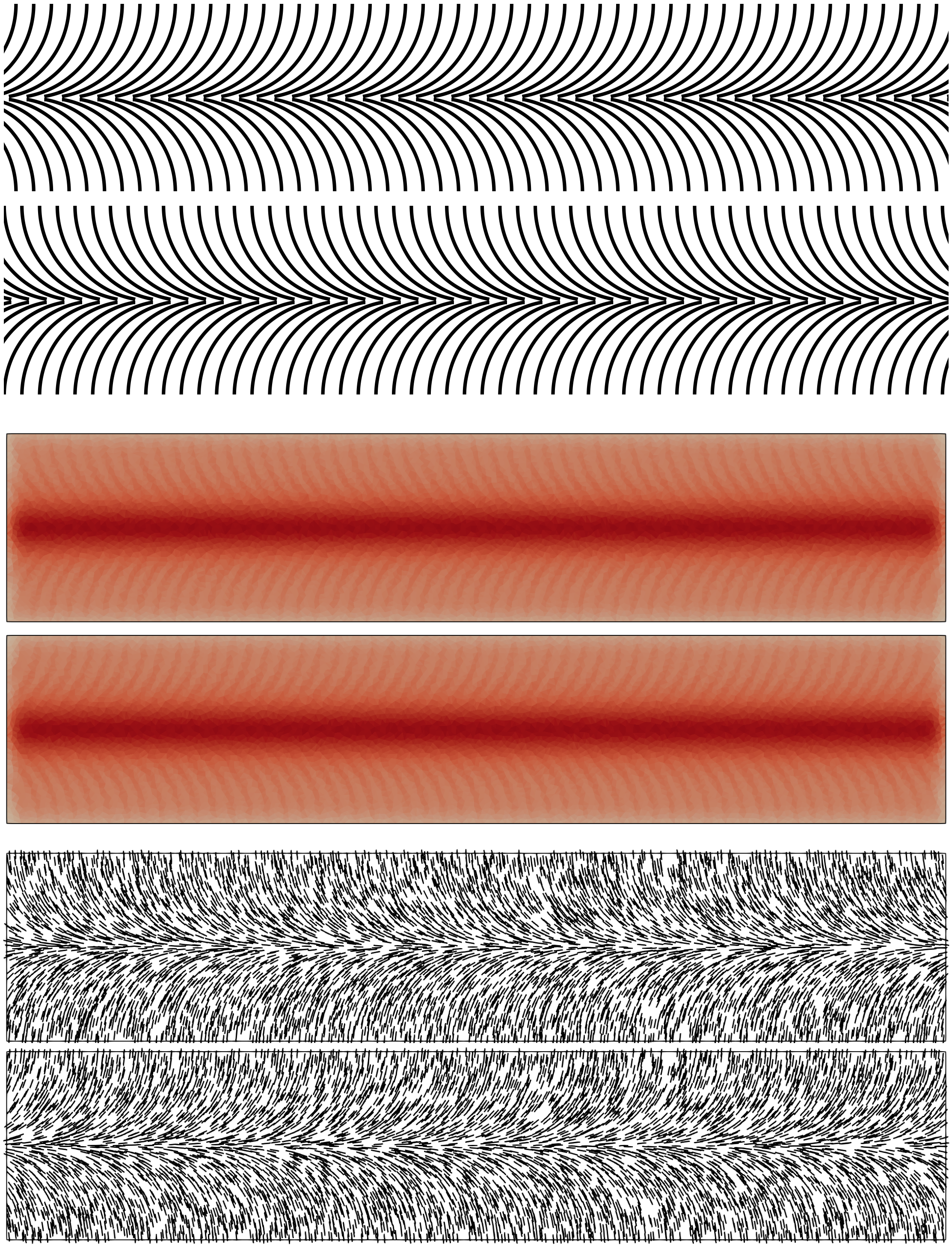

Figure S3: Details of the catenoid. For each of the bottom/top layer, we show the experimental print path (top), the numerical density field (middle) and the numerical filament-tangential growth direction (bottom).

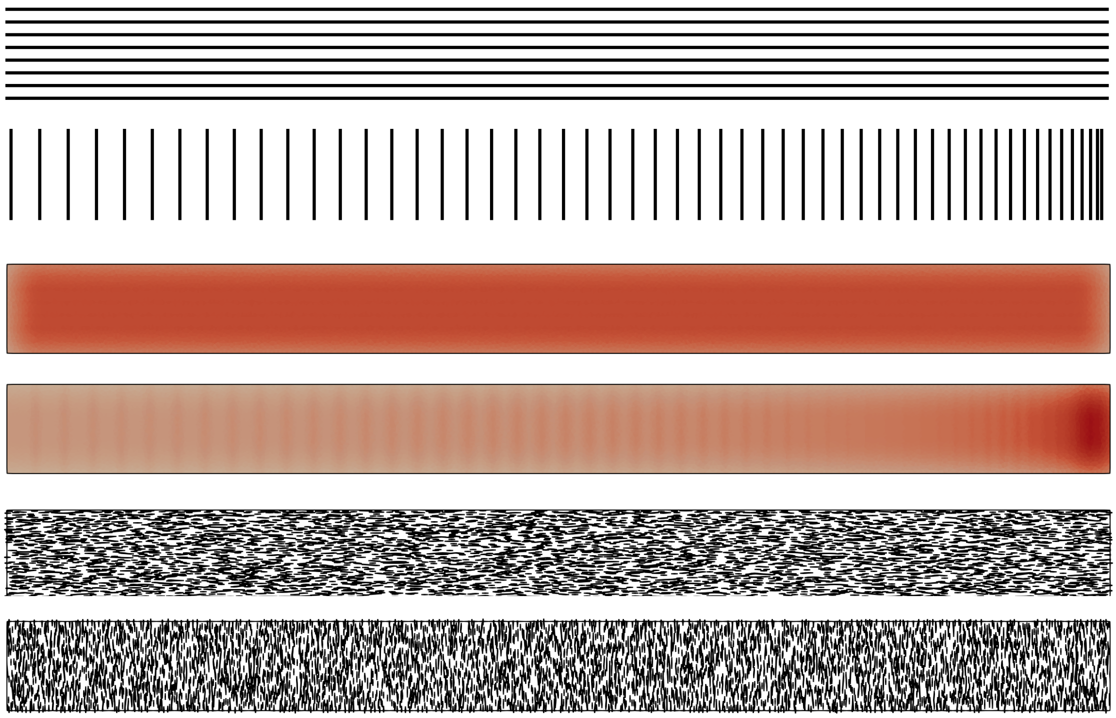

Figure S4: Details of the logarithmic spiral. For each of the bottom/top layer, we show the experimental print path (top), the numerical density field (middle) and the numerical filament-tangential growth direction (bottom).

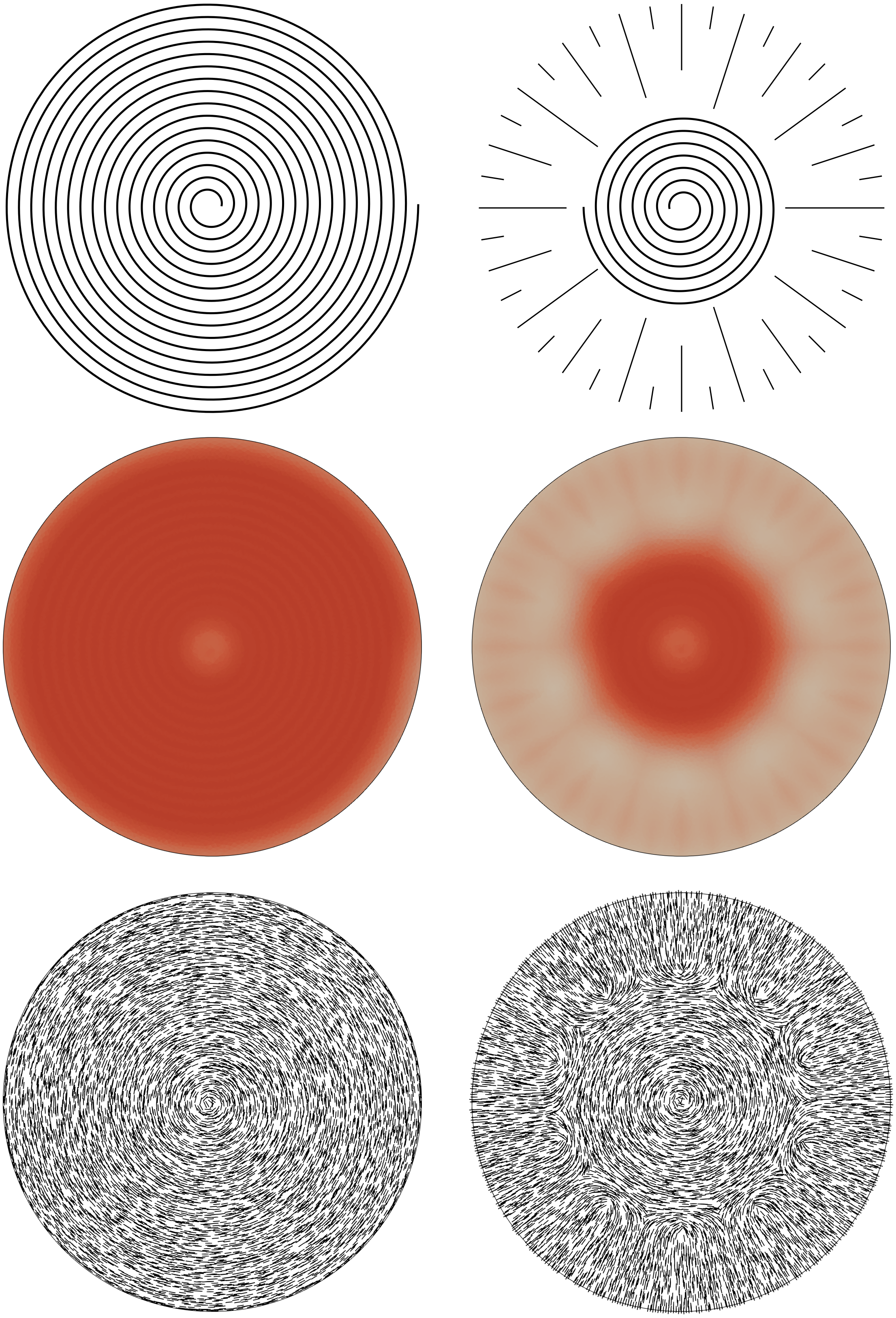

Figure S5: Details of the sombrero. For each of the bottom/top layer, we show the experimental print path (top), the numerical density field (middle) and the numerical filament-tangential growth direction (bottom).

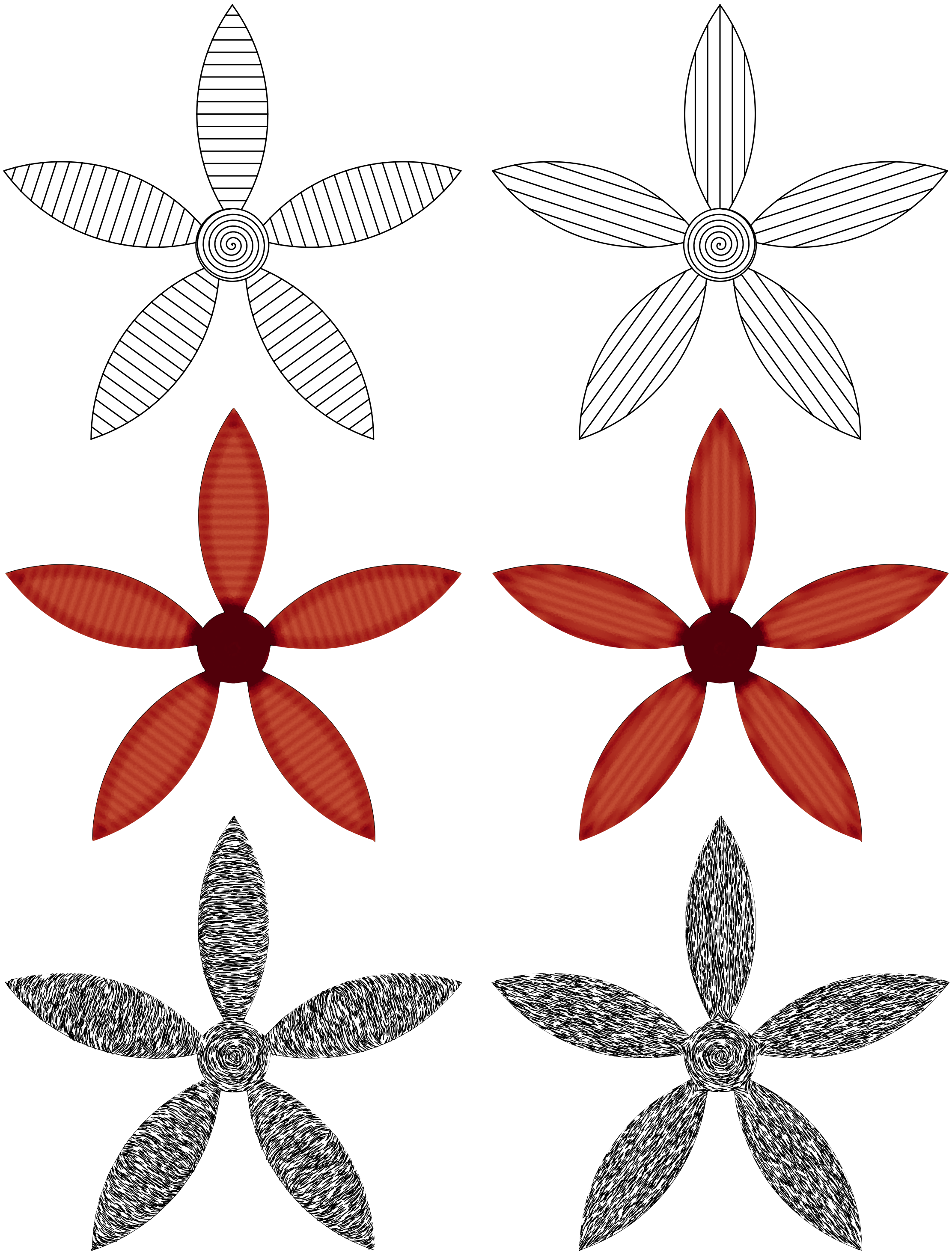

Figure S6: Details of the folding flower. For each of the bottom/top layer, we show the experimental print path (top), the numerical density field (middle) and the numerical filament-tangential growth direction (bottom).

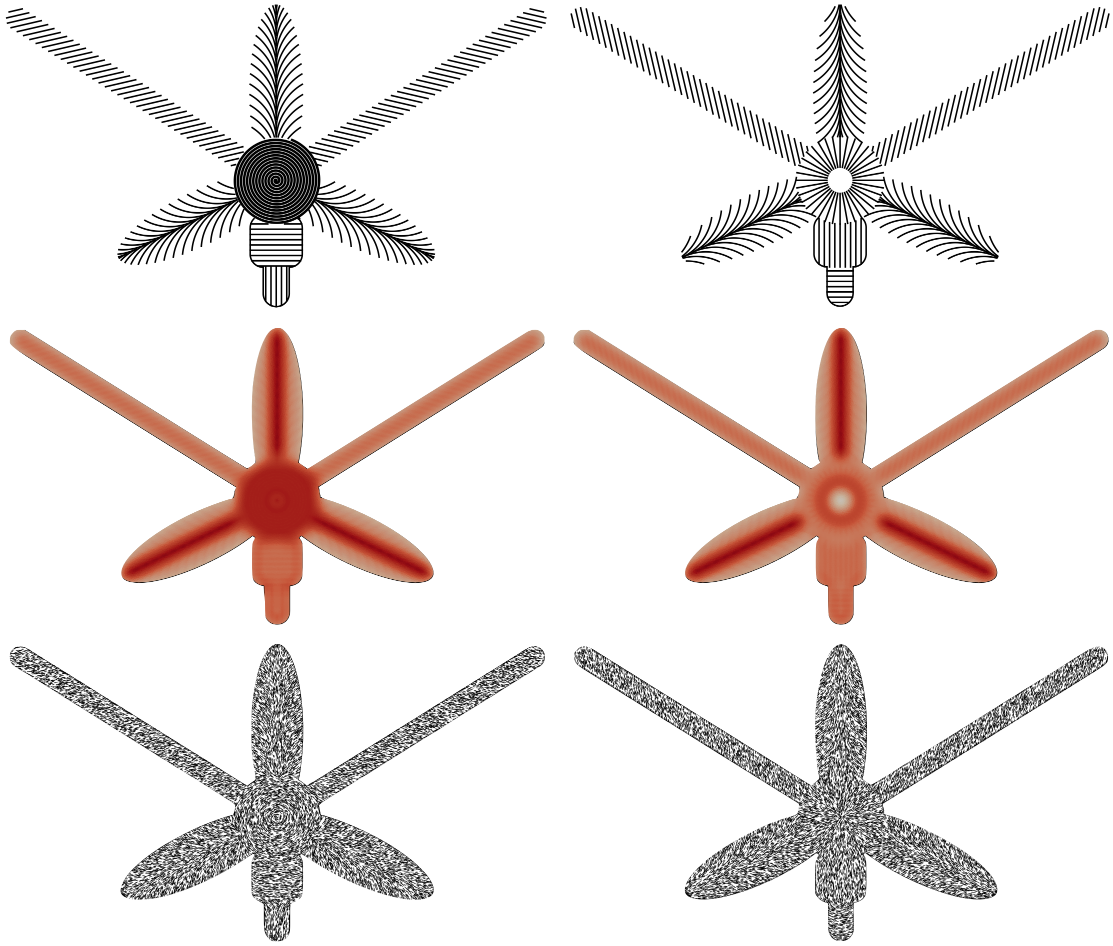

Figure S7: Details of the orchid. For each of the bottom/top layer, we show the experimental print path (top), the numerical density field (middle) and the numerical filament-tangential growth direction (bottom).

S3 Computational details

In table S1 we report the number of triangles (N_T) and average number of evaluations for each quasi-static minimization step (N_m) for all the test cases reported in this work.

All simulations were run on a Linux workstation with an Intel Xeon Gold 6130 CPU with 64 GB internal memory, and took between several minutes for the sombrero to about a day for the catenoid, while sharing the computational resources of the workstation between two to three simulations.

Table S1: Computational settings for the different test cases simulated here. The columns represent number of triangles (N_T) and the average number of function evaluations for each quasi-static minimization step (N_m).

case	N_T	N_m
helicoid	12 430	22 355
catenoid	12 430	655 903
logarithmic spiral	12 415	327 407
sombrero	18 776	10 243
folding flower	15 185	55 895
orchid	28 870	118 849

S4 Orchid mid-surface strains

We represent the mid-surface stretching strains on each triangle T using a scalar quantity $\varepsilon_T = \sqrt{\left\|(\mathbf{a}_r)_T^{-1}(\mathbf{a}_c)_T - \mathbf{I}\right\|_{e,T}^2}/Y_T$. Plotting this quantity over the mid-surface of the final orchid geometry in figure S8. This distribution shows the large strains at the lower locations where the large petals connect to the center disk. A careful inspection of the experimental sample (see main text) shows that this is exactly the location where structure failure occurs.

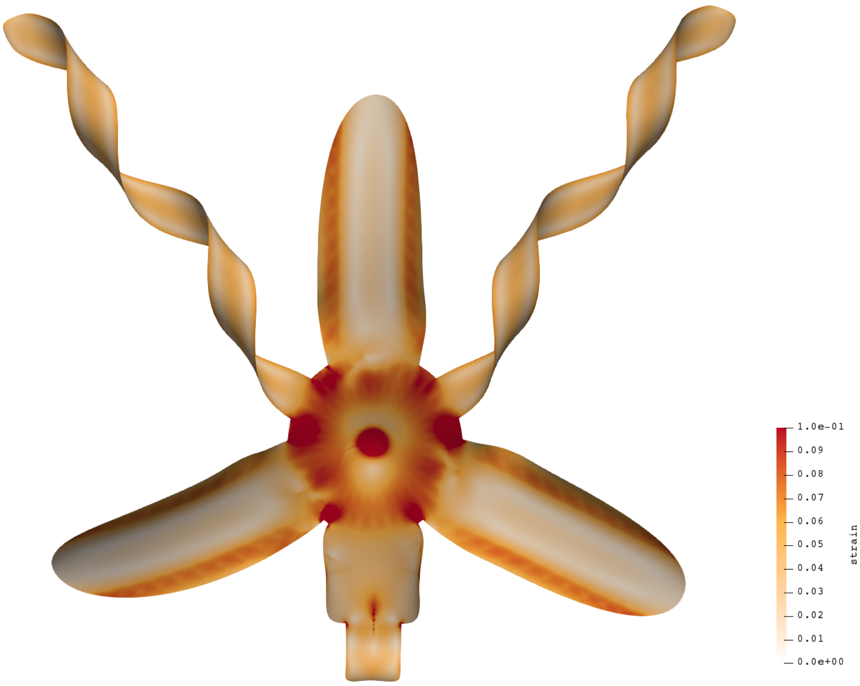

Figure S8: Distribution of mid-surface stretching strains ε plotted in the grown state.

References

[1] E. Efrati, E. Sharon, and R. Kupferman. Elastic theory of unconstrained non-Euclidean plates. *Journal of the Mechanics and Physics of Solids*, 57(4):762–775, 04 2009.

[2] A. Sydney Gladman, Elisabetta A. Matsumoto, Ralph G. Nuzzo, L. Mahadevan, and Jennifer A. Lewis. Biomimetic 4D printing. *Nature Materials*, 15(4):413–418, January 2016.